Ultra-short pulsed Laser Ablation of Indium Tin Oxide with GHz and MHz Bursts

Sönke Vogel*1, Benedikt Bornschlegel1, Marius Dahmen2, Sabrina Vogt2, and Christian Hinke1

¹Chair for Laser Technology (LLT), RWTH Aachen University, Germany

²Saint-Gobain Research Germany

*Corresponding author's e-mail: soenke.vogel@ilt.fraunhofer.de

Indium Tin Oxide (ITO) is widely used material for example in displays or solar cells. In this work we focused on increasing the productivity and processing quality of ultra-short pulsed laser ablation of ITO with MHz and GHz bursts. Thick ITO films could not be ablated with one pulse, preventing optical stamping. With MHz bursts thick (200 nm) ITO films could be completely removed with one burst. Moreover, the ridge height around the ablated lines were diminished. On the other hand, GHz bursts could not completely remove the ITO film. Ablation with bursts with tens of sub-pulses result in ablation results in increasing ridge height. With MHz bursts the productivity and quality could be greatly enhanced.

DOI: 10.2961/ilmn.2025.03.2011

Keywords: Indium Tin Oxide, burst, ultra-short pulsed, GHz burst, MHz burst

1. Introduction

Indium tin oxide (ITO) owns its popularity amongst multiple applications to its high transparency in the visible regime with simultaneously high electrical conductivity. Ultra-short pulsed (USP) laser ablation enables precise processing of wide-band gap materials such as ITO. Therefore, USP laser micro-machining of ITO thin films has been extensively studied. However, USP laser micro-machining is still restrained by its lack of productivity. Three approaches, in particular, high repetition rate lasers in conjunction with fast beam deflection methods, parallel processing with multiple beams or pulse bursts are utilized to improve productivity.

In most studies of ITO USP laser ablation, full removal of a thicker ITO film (>100 nm) could only be attained with multiple pulses [1–4]. However, the need for multiple pulses excludes single shot ablation on the fly with shaped beams [5]. On the other hand, substrate side ablation facilitates a complete removal, even of thicker ITO films, with one pulse [4,6,7]. But at the same time, high ridges have been reported [7–9]. In conclusion, a combination of low ridges and a complete film ablation with a single pulse is preferential, enabling optical stamping or fast beam deflection.

The bandgap of ITO ranges between 3.5 eV to 4.2 eV and the equilibrium free charge carrier density ranges in the order of 10^{20} cm⁻³ to 10^{21} cm⁻³ [10–12] and depends in the tin doping content. Owing to the doping, new energy levels, overlapping with the conduction band, are introduced. For ITO cascade ionization dominates multiphoton absorption [11,13]. Hence, a fast free carrier generation in response to laser irradiation increases the reflectivity within the ultrashort pulse duration [7,8,11]. By electron-lattice coupling a liquid-gas mixture forms at around few tens of picoseconds [7–9], rendering the irradiated area absorptive in pump-prober experiments. At around 100 ps the film starts to bulge at the crater's edge. The crater's center remains dominated by the liquid-gas mixture up to a few hundreds of

picoseconds for lower peak fluences and up to 1 ns for higher fluences. For higher delay times a disintegration of the film was observed. [7,8]

Double pulse ablation studies with various time delays showed shielding and even material re-deposition [14–18], deemed the "valley of death". It ranges from ca. 100 ps to several hundreds of picoseconds for various metals. For MHz burst laser ablation of copper and aluminum an oscillating volume efficiency has been reported, with local maxima for odd number of pulses in a burst [19-26] but not for steel [23-25]. For GHz burst an efficiency increase is explained by heat accumulation [27-30]. Förster et. al. [18] have summarized multiple studies with different number of pulses per burst (PPB). For a smaller PPB (<30) shielding decreases the energy specific volume. For several tens to hundreds of pulses the energy specific volume increases. MHz burst are additionally used for polishing [31–34]. For dielectrics an increase in ablation efficiency for GHz and MHz burst was reported [35–38].

2. Materials & Methods

An ITO (180 nm, $10~\Omega/\Box$) thin film on soda-lime glass with an intermediate SiO_2 passivation layer was purchased from Präzisions Glas & Optik GmbH and was used for all experiments. The film thickness was validated by transmission electron microscopy. Transmission and reflectance spectra were measured and the Tauc-Lorentz-Drude model for the susceptibility was fitted with the transfer matrix method [39,40] to the data. The real and imaginary part of the susceptibility as well as the electron-mobility ,-density, film thickness and the band gap were determined. The formula for the Tauc model is given in [41].

The experiments were conducted with a 1030 nm ultrashort pulsed (USP) laser (Carbide, Light Conversion) at 300 fs with a measured beam diameter of 24.1 μm . The inter-pulse delay within a burst train for GHz and MHz bursts is 400 ps and 16 ns, respectively. The utilized burst fluences

were selected such that the sub-pulse fluences are comparable across different burst lengths The burst fluences range from below the ITO single pulse threshold fluence to 20 J/cm². Up to 25 PPB were used for GHz burst ablation and up to 15 for MHz burst ablation. For steady state results up to 200 pulses were shot at the same location with a repetition rate of 1 kHz in order to suppress heat accumulation.

Topography measurements were conducted with a white light interferometer (NewView NX, Zygo) and an atomic force microscope (AFM, N8 RADOS, Bruker nano GmbH). The depth was determined according to EN ISO 5436 A2 [42] and the width from profiles along the crater's short axis around 5 nm below the reference surface. Ten pulses were averaged. Threshold fluences ϕ_{Th} and effective diameters ω_{eff} were determined by Liu's method [43]. Volumes were determined from the measured topography. In conductive thin film ablation a galvanic separation is the aim of the process. It is achieved by completely removing the conductive thin film. Therefore, an additional measure besides the volume efficiency is used - the depth efficiency (DE). The volume efficiency peaks at $e^2 \cdot \phi_{Th}$. The optimum fluence with respect to the DE is $e \cdot \phi_{Th}$.

For MHz bursts and steady state results the transmitted energy of each pulse is measured with an integrating sphere (2P3/M, Thorlabs), a photodiode (PDA10A2, Thorlabs) and an oscilloscope (PS6452, PicoScope). 75 % pulse overlap was chosen for line ablation. The necessary scan speed was calculated from the measured single spot ablation crater diameters for each parameter set. A repetition rate of 200 kHz was used. The threshold fluence of the glass substrate is 3.1 J/cm².

3. Results

3.1 Material Characterization

The optical fit as well as the electron transmission microscopy measurement confirms the film thickness of 180 nm (Fig. 14).

Table 1 Calculated ITO properties from Tauc-Lorentz-Drude model fit.

Property	Value	
Band gap	3.5 eV	
thickness	175 nm	
Electron mobility	12.8 Ωcm ⁻¹	
Sheet resistance	10 Ω/□	

3.2 Steady State Ablation

For steady state ablation, the threshold fluence does not change for ablation with 1 to 5 pulses. For ablation with 6 or higher PPB, the threshold fluence slightly decreases. The crater diameters do not change with the number of incident pulses. For higher fluences up to 12 J/cm² the film cannot be removed with a single pulse. The DE decreases with an increasing total fluence (Fig. 12). The DE slightly increases with the number of pulses.

The measured transmission decreases with the fluence (Fig. 11). The reflection and absorption increase. The decrease is independent of the number of previous pulses. For fluences greater than 0.8 J/cm² and from two pulses onwards the formation of LIPSS is observed (Fig. 4). A blueish

concentric region around the crater and at low fluences was measured by AFM (Fig. 1). It is neither a modification nor a delamination nor a heat affected zone. It is a partial ablation of ITO grains. Moreover, the material was partially melted and re-solidified, indicated by the droplets.

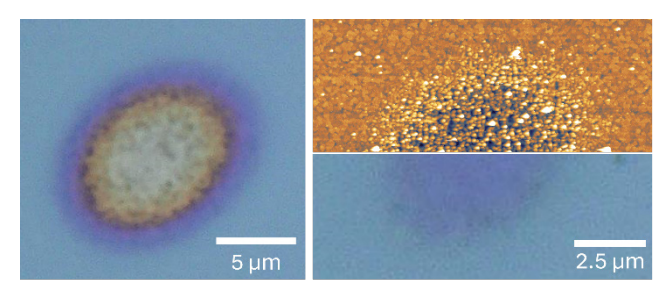


Fig. 1 Microscope images of an ablation crater ablated with 4 pulses with a pulse fluence of 0.45 J/cm² at 1 kHz and for 3 pulses at 0.33 J/cm² (right, bottom) and the respective AFM image (right, top).

3.3 GHz Burst Ablation

A slightly higher volume efficiency is noticed for the same number of pulses as compared to the steady state ablation. For 5 and 6 pulses the DE exceeds the DE of the steady state case and reaches its maximum of 15 nm/μJ at 1.2 J/cm² for >7 PPB. The DE then decreases with increasing fluences. The DE remains below the single pulse case for bursts with <5 PPB for all fluences. The diameter is larger than for the steady state case. It approaches the single pulse ablation case with the same fluence as the sum of the individual pulse fluences. No LIPSS formation is observed.

The depth changes stepwise (Fig. 2). For 2 to 5 pulses multiple steps are observable. The steps are pronounced and the depths do not increase until a significant higher fluence is incident. The sub-pulse threshold fluence decreases with the number of PPB.

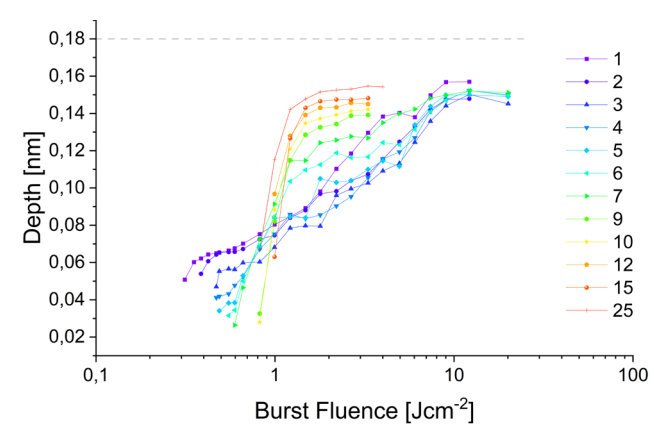


Fig. 2 Ablation depth with GHz bursts with increasing number of PPB.

3.4 MHz Burst Ablation

The single pulse threshold fluence decreases with the number of PPB. The volume efficiency for 5 pulses within a MHz burst is higher than the steady state or GHz burst case. Further analysis of the DE for higher PPB (>15) was not possible because the film was completely ablated. The DE exceeds the steady state case at 0.8 J/cm². The maximum DE is located at ca. 1.2 J/cm² for up to 7 PPB and shifts to higher total fluences for higher PPB numbers. No pronounced

stepwise depth increase is observed with regards to the total fluence.

For total fluences below the burst threshold fluence, an uplift of the ITO film is observed and cracks forming in the center of the uplift. The formation of LIPSS cannot be confirmed with certainty. For higher fluences, structures parallel to the polarization direction exist.

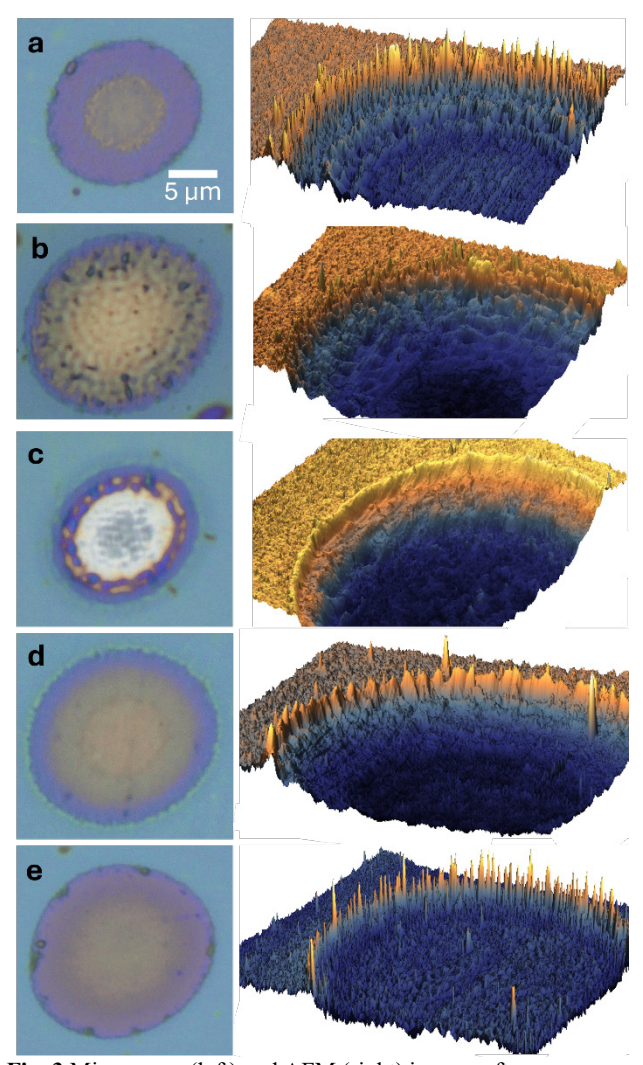


Fig. 3 Microscope (left) and AFM (right) images after a) GHz burst with 3 PPB at 1 J/cm² and a depth of 75 nm

- b) MHz burst with 2 PPB at 2.2 J/cm² and a depth of 110 nm
- c) MHz burst with 5 PPB at 1.85 J/cm², depth = 177 nm
- d) GHz burst with 7 PPB at 1.2 J/cm², depth = 114 nm
- a) of 12 burst with / 11 b at 1.2 J/cm , depth = 11
- e) a single pulse at 1.2 J/cm^2 , depth = 85 nm.

The transmission decreases with increasing fluence for all sub-pulses within a burst. The transmission decreases with each subsequent sub-pulse within the burst. The reflection was not measured. For fluences lower than the single pulse threshold fluence, a decrease in transmission is observable for subsequent pulses.

3.5 Line Ablation

For lines processed with single pulses and a pulse overlap of 75 % at a repetition rate of 200 kHz the threshold fluence decreases compared to single pulse ablation. Even at the lowest burst fluence ITO is completely removed for the examined MHz burst cases (2 PPB and 5 PPB). In the GHz case (7 PPB) the ITO is only considered fully removed above 3.3 J/cm^2 .

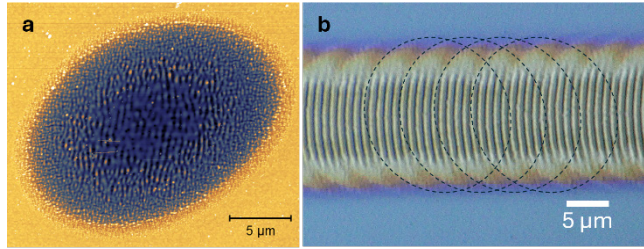


Fig. 4 a) Formation of LIPSS for 3 pulses at 1 kHz and 0.9 J/cm². **b)** LIPSS in a scanned line with 200 kHz, 75 % pulse overlap, 0.6 J/cm² and 2 PPB in a MHz burst. The special frequency of the LIPSS is 941.3 nm. Dashed lines guide the eye to find the outline of individual craters.

Very noticeable LIPSS are observed for all cases except for the GHz burst case (Fig. 4). The line width for the burst cases is larger than for the single pulse case at the same subpulse fluence but smaller than the single pulse case at the same total fluence.

Table 2 Line width for constant burst/pulse fluence and constant sub-pulse fluence.

fluence [J/cm ²]	width [μm]				
sub-pulse	1 pulse width	MHz 2 PPB	MHz 5 PPB	GHz 7 PPB	
0.25	9.7	11.6	17.0	21.7	
total					
0.83	19.2	15.9	13.8	15.6	

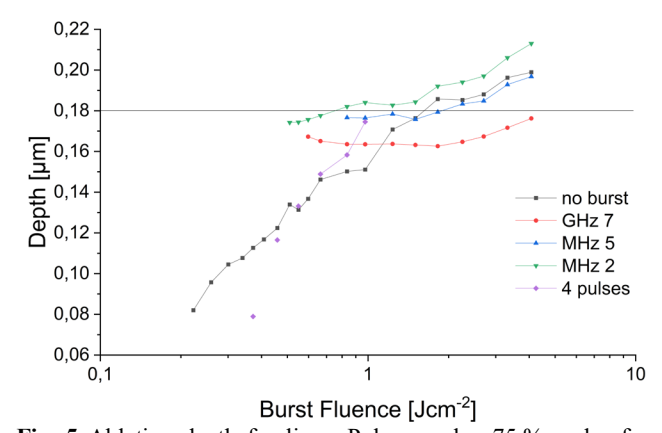


Fig. 5 Ablation depth for lines. Pulse overlap 75 %, pulse frequency 200 kHz. For comparison single pulse ablation results for 4 pulses with a repetition rate of 1 kHz are shown.

4. Discussion

In general results from e.g. 2 PPB and 3 PPB are not completely comparable since the energy per single pulse varies (Fig. 13).

Steady State Ablation

The increase in reflection is attributed to a rapidly generated free electron plasma which is significantly more reflective. At the same time the electron plasma is more

absorptive and therefore the measured transmission decreases. No significant change in transmission with the number of pulses is observed (Fig. 10), even though the remaining ITO becomes thinner after each pulse. The transmission decreases for fluences below the threshold fluence. This decrease is attributed to multi-photon absorption and measured by the z-scan method [44]. For all cases, steady state, GHz bursts or MHz burst, the first pulse is the most efficient in terms of volume removal per incident energy. Every additional incident pulse removes roughly the same amount of volume V_{pulse} for a constant sub-pulse fluence ϕ . The first pulse however removes $V_{pulse} + V_{initial}$. Therefore, the volume efficiency asymptotically trends towards

$$\lim_{n \to \infty} \frac{n \cdot V_{pulse} + V_{initial}}{n \cdot \phi} = \frac{V_{pulse}}{\phi}.$$
 (1)

The existence of an initial volume $V_{initial}$, caused by a minimum ablation depth, has been noted [45] and the Furmanski model [46] was updated.

GHz Burst Ablation

The depth efficiency is lower than the single pulse ablation efficiency for up to 6 PPB. The DE then increases for higher burst fluences. This effect has been observed before as mentioned in 1. For higher fluences the film is never completely ablated. At higher sub-pulse fluences shielding limits further energy deposition. For lower burst fluences (<0.8 J/cm²) shielding dominates the heat accumulation and the DE is lower than for the steady state case.

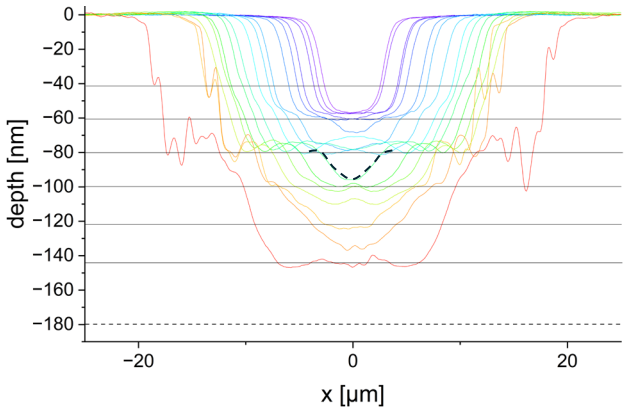


Fig. 6 Ablation crater cross sections measured by white light interferometry for a MHz burst with 5 PPB. An example for a parabolic "sub-crater" is highlighted by a dashed line.

The very pronounced stepwise change in depth with regards to the fluence is only present for ca. up to 9 PPB. For higher PPB numbers the sub-pulse fluence has dropped below the single pulse threshold fluence in the examined range. The stepwise depth change might be associated with the shielding by an absorbing fluid-gas layer. The energy is mostly absorbed in the fluid-gas layer which is than expelled in a spallation event. Only if the transmitted fluence than exceeds a critical fluence, a "sub-crater" with a parabolic shape forms (Fig. 6). Multiple spallations, also for single pulse ablation, and the formation of "sub-craters" have been observed before [7,8,45]. The ridge height increases further for higher PPB (>6). This indicates a more violent ablation event. We hypothesize that lower sub-pulse fluences have a penetration depth closer to an un-irradiated film (10.4 μm).

Therefore, the whole film is thermalized further with each sub-pulse and then it disintegrates rapidly, creating high ridges. At lower PPB the sub-pulse fluences are high enough to induce spallation, which in turn generates higher ridges.

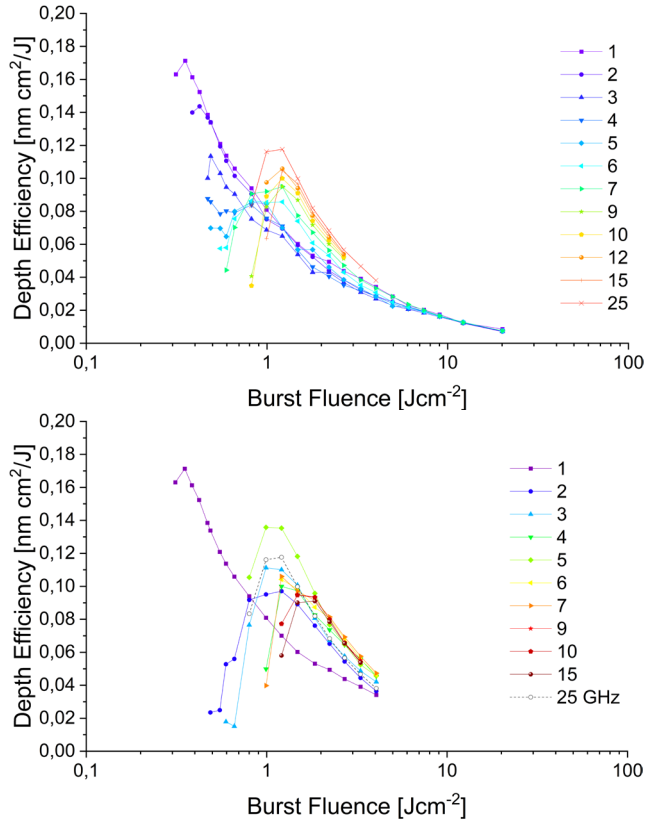


Fig. 7 depth efficiency for GHz bursts (top), MHz bursts (bottom).

MHz Burst Ablation

As for the GHz burst case, the DE is lower as the steady state case for lower fluences and then exceeds the steady state case above 0.8 J/cm². The DE is not noticeably higher than for GHz bursts. However, MHz bursts are able to fully remove the ITO film. But for 2 and 3 PPB a pronounced DE decrease as compared to GHz bursts is observed. The spalled film might be redeposited. The DE oscillates with the number of PPB, having local maxima at odd PPB numbers. However, the highest DE is found at 5 PPB, whereas aluminum or copper typically have a volume efficiency maximum at 3 PPB. 3 PPB might be less efficient because they also seem to be limited in depth at around 150 nm as observed for GHz bursts. For all PPB numbers the DE maximum is found at 1.2 J/cm². For 3 PPB this results in a higher sub-pulse fluence as compared to 5 PPB. Therefore, the higher reflectivity increase might limit a more efficient ablation at 3 PPB. Even PPB numbers clear the ablation plume and therefore have lower DE.

For higher PPB numbers the same explanation for increasingly higher ridges is considered as for GHz bursts: the sub-pulses thermalize the film and then a rapid phase explosion might occur. For lower PPB numbers the ridge height is diminished. The ridges might be shattered by redeposited particles and scattered radiation or sub-threshold melting and re-solidification (Fig. 3). For lower PPB numbers the material is fully ablated before the next sub-pulse. Therefore, the radiation is not absorbed by a liquid-gas mixture as for

the GHz case and can penetrate deeper into the material, resulting in a superior film removal.

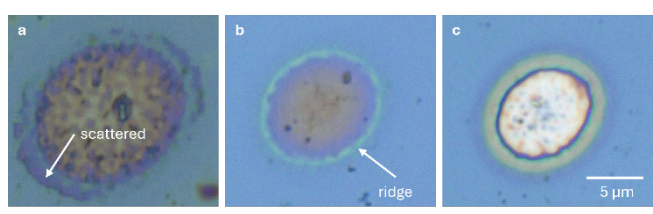


Fig. 8 a) ablation crater with MHz burst, 2 PPB at 1.2 J/cm² b) GHz burst with 12 PPB at 1.2 J/cm² c) MHz burst, 12 PPB at 1.85 J/cm².

5. Conclusion

The single pulse threshold fluences for all bursts decrease with an increasing number of PPB. The decrease is in accordance with the incubation theory. From the steady state experiments we conclude that persistent material modification, such as the introduction of color centers do not contribute significantly to the decrease of the sub-pulse threshold fluence observed for bursts. Multi-photon absorption in ITO is less important in supplying free electrons. ITO is doped and free electrons are already present [11]. Therefore, we assume that heat accumulation is the driving process behind the threshold fluence decrease. For longer inter-pulse delays, the material cools further down. Therefore, a higher incubation factor was measured for GHz bursts as compared to MHz bursts. For lower sub-pulse fluences, coinciding with more PPB, we hypothesize that a full thermalization of the film leads to a rapid ablation.

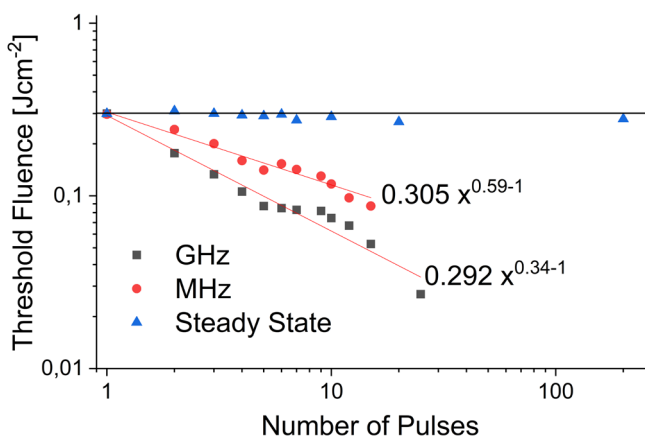


Fig. 9 Burst threshold fluence for bursts with different numbers of PPB. The steady state case was produced with 1 kHz. The black line highlights the single pulse threshold fluence. An incubation model was fitted.

More PPB have been compared to nanosecond ablation [18]. The same is thought to be applicable for ITO. With MHz bursts a full film removal is possible. MHz bursts up to 3 sub-pulses reduce the ridge height. With GHz bursts a full film removal is not possible even for high sub-pulse fluences and 25 PPB. This is attributed to shielding by a liquidgas mixture. More PPB result in higher ridges, resembling nanosecond ablation results. With MHz bursts, especially with 2 and 3 PPB, ridge free lines could be fully ablated. The line width is reduced as compared to single pulse ablation.

Overall MHz burst ablation for ITO thin films seems very promising. Multiple issues are solved at once. First, a

full removal even of thick ITO films is possible with one burst, enabling optical stamping. Second, ridges have been almost completely suppressed for 2 to 4 PPB. Third, the depth efficiency is increased, enabling faster processing speeds.

Acknowledgements

Funded by the Deutsche Forschungsgemeinschaft (DFG, German Research Foundation) under Germany's Excellence Strategy – EXC-2023 Internet of Production – 390621612. This research is funded by the Digital Photonic Production DPP Research Campus as part of the "Research Campus Public-Private Partnership for Innovation" research funding initiative of the German Federal Ministry of Education and Research (BMBF). (Funding number: 13N15423)

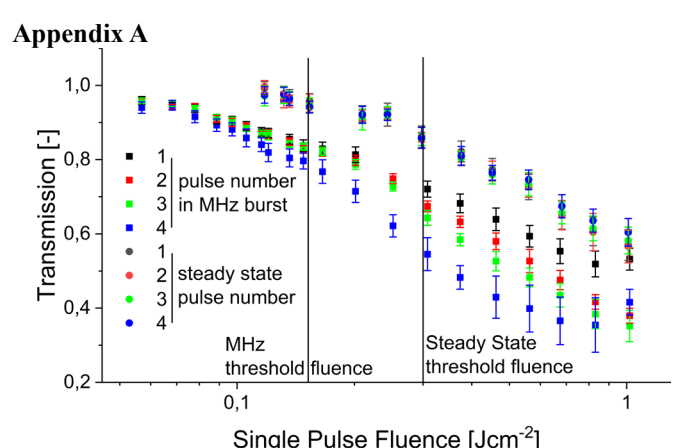


Fig. 10 Measured transmission for each sub-pulse within a MHz burst train and for four steady state pulses. The fluences are the pulse or sub-pulse fluences.

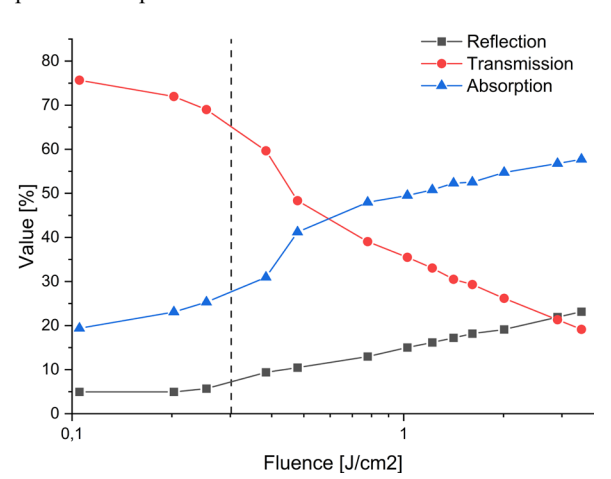


Fig. 11 transmission (T) and reflection (R) measurement for a single pulse ITO ablation with increasing fluences. Absorption was calculated by 100-R-T. The dashed line represents the threshold fluence.

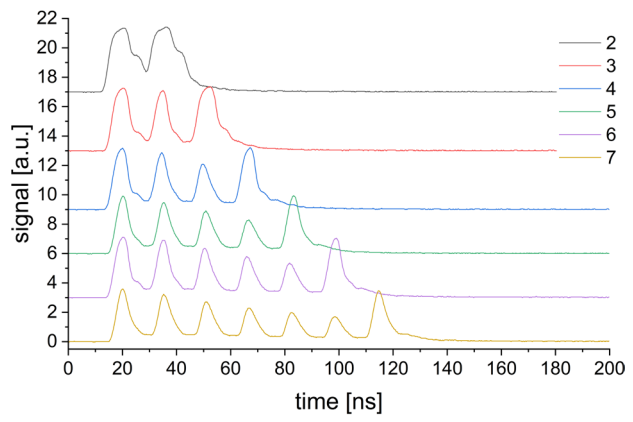


Fig. 13 Measured sub-pulse photodiode response of a MHz burst train with different PPB numbers.

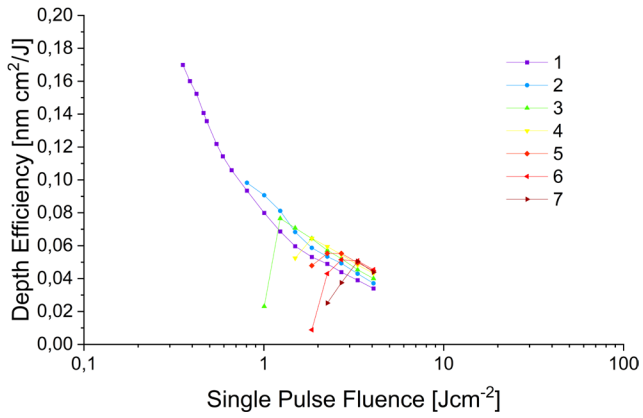


Fig. 12 Depth efficiency for the steady ablation. The depth efficiency decreases with an increasing fluence.

References

- N. Farid, H. Chan, D. Milne, A. Brunton, and G. M. O'Connor: Appl. Surf. Sci., 427, (2018) 499.
- [2] J. Köller, A. Sassmannshausen, M. Kratz, and J. Voß: J. Laser Micro Nanoeng, 17, (2022) 174.
- [3] C. Y. Leong, S. S. Yap, G. L. Ong, T. S. Ong, S. L. Yap, Y. T. Chin, S. F. Lee, T. Y. Tou, and C. H. Nee: Nanotechnol. Rev., 9, (2020) 1539.
- [4] P. Liu, W. Wang, X. Mei, B. Liu, and W. Zhao: Opt. Lasers Eng., 69, (2015) 35.
- [5] P. M. Harrison, N. Hay, and D. P. Hand: Appl. Surf. Sci., 256, (2010) 7276.
- [6] S. Krause, P. T. Miclea, F. Steudel, S. Schweizer, and G. Seifert: EPJ Photovolt., 4, (2013) 40601.
- [7] G. E. Hallum, D. Kürschner, C. Eulenkamp, R. Auer, B. Hartmann, W. Schulz, and H. P. Huber: Opt. Express, 31, (2023) 43017.
- [8] G. E. Hallum, D. Kürschner, D. Redka, D. Niethammer, W. Schulz, and H. P. Huber: Opt. Express, 29, (2021) 30062.
- [9] C. McDonnell, D. Milne, H. Chan, D. Rostohar, and G. M. O'Connor: Opt. Lasers Eng., 81, (2016) 70
- [10] J. Du, X. Chen, C. Liu, J. Ni, G. Hou, Y. Zhao, and X. Zhang: Appl. Phys. A, 117, (2014) 815.
- [11] D. Kürschner, G. Hallum, S. Vogel, H. P. Huber, and W. Schulz: Int. J. Heat Mass Transfer, 209, (2023) 124119.
- [12] L. W. van Beveren, E. Panchenko, N. Anachi, L. Hyde, D. Smith, T. D. James, A. Roberts, and J. C.

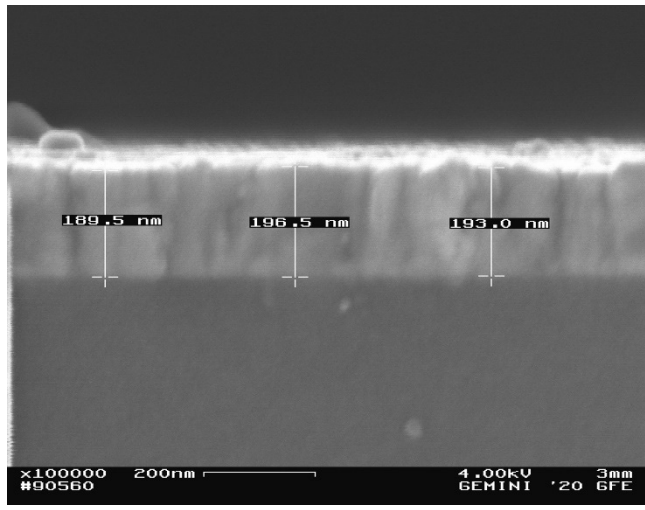


Fig. 14 Transmission electron microscope image of a sample from the batch used for the experiments in this study.

- McCallum: 2014 Conf. Optoelectronic Microelectron. Mater. Devices (COMMAD), (2014) 144.
- [13] L. V. Keldysh: Sov. Phys. JETP, 20, (1965) 1307.
- [14] M. Spellauge, J. Winter, S. Rapp, C. McDonnell, F. Sotier, M. Schmidt, and H. P. Huber: Appl. Surf. Sci., 545, (2021) 148930.
- [15] D. J. Förster, S. Faas, S. Gröninger, F. Bauer, A. Michalowski, R. Weber, and T. Graf: Appl. Surf. Sci., 440, (2018) 926.
- [16] Masaki Hashida, Shinichiro Masuno, Yuki Furukawa, Shogo Nishino, Mitsuhiro Kusaba, Shunsuke Inoue, Shuji Sakabe, Hitoshi Sakagami, and Masahiro Tsukamoto: Proc SPIE, Vol. 10522, (2018) 105220S.
- [17] S. Noël and J. Hermann: Appl. Phys. Lett., 94, (2009).
- [18] D. J. Förster, B. Jäggi, A. Michalowski, and B. Neuenschwander: Materials, 14, (2021) 3331.
- [19] A. Žemaitis, P. Gečys, M. Barkauskas, G. Račiukaitis, and M. Gedvilas: Sci. Rep., 9, (2019) 12280.
- [20] A. Žemaitis, M. Gaidys, P. Gečys, and M. Gedvilas: Sci. Rep., 14, (2024) 5614.
- [21] T. Kramer, B. Neuenschwander, B. Jäggi, S. Remund, U. Hunziker, and J. Zürcher: Phys. Procedia, 83, (2016) 123.
- [22] T. Kramer: J. Laser Micro/Nanoeng., 12, (2017) 107.
- [23] A. Žemaitis, M. Gaidys, P. Gečys, M. Barkauskas, and M. Gedvilas: Opt. Express, 29, (2021) 7641.
- [24] B. Bornschlegel, M. Kratz, and J. Finger: J. Laser Micro Nanoeng, 17, (2022) 19.
- [25] B. Bornschlegel and D. Haasler: J. Laser Micro Nanoeng, 19, (2024) 57.
- [26] B. Neuenschwander, T. Kramer, B. Lauer, and B. Jäggi: Proc. SPIE, Vol. 9350, (2015) 93500U.
- [27] S. Bruening, K. Du, and A. Gillner: Procedia CIRP, 94, (2020) 856.
- [28] H. Matsumoto, Z. Lin, and J. Kleinert: Proc. SPIE, 10519, (2018) 1051902.
- [29] M. E. Povarnitsyn, P. R. Levashov, and D. V. Knyazev: Appl. Phys. Lett., 112, (2018) 051603.
- [30] G. Bonamis, E. Audouard, C. Hönninger, J. Lopez, K. Mishchik, E. Mottay, and I. Manek-Hönninger: Opt. Express, 28, (2020) 27702.

- [31] M. Osbild, A. Brenner, L. Röther, and J. Finger: Procedia CIRP, 94, (2020) 936.
- [32] A. Brenner, L. Röther, M. Osbild, and J. Finger: Proc. SPIE, Vol. 11268, (2020) 112680P.
- [33] A. Michalowski, F. Nyenhuis, and G. Kunz: PhotonicsViews, 17, (2020) 42.
- [34] D. Metzner, P. Lickschat, and S. Weißmantel: Appl. Surf. Sci., 531, (2020) 147270.
- [35] N. Hodgson, H. Allegre, and Starodoumov: J. Laser Micro Nanoeng, 15, (2020) 236.
- [36] S. Schwarz, S. Rung, C. Esen, and R. Hellmann: Opt. Lett., 46, (2021) 282.
- [37] S. T. Hendow, H. Takahashi, M. Yamaguchi, and J. Xu: Proc. SPIE, Vol. 11268, (2020) 1126809.
- [38] S. M. Remund, M. Gafner, M. V. Chaja, A. Urniezius, S. Butkus, and B. Neuenschwander: Procedia CIRP, 94, (2020) 850.
- [39] C. C. Katsidis and D. I. Siapkas: Appl. Opt. 41, (2002) 3978.
- [40] B. Harbecke: Appl. Phys. B, 39, (1986) 165.
- [41] J. Tauc: Mater. Res. Bull., 3, (1968) 37.
- [42] International Organization for Standardization: DIN EN ISO 5436, (2000).
- [43] J. M. Liu: Opt. Lett., 7, (1982) 196.
- [44] A. Tognazzi, P. Franceschini, T. N. L. Tran, A. Chiasera, M. A. Vincenti, A. C. Cino, N. Akozbek, M. Scalora, and C. de Angelis: Adv. Opt. Mater, 19, (2023) 100242.
- [45] D. Redka, S. Vela, M. Spellauge, J. Minár, M. Morales, C. Molpeceres, and H. P. Huber: Opt. Laser Technol., 189 (2025), 113103.
- [46] J. Furmanski, A. M. Rubenchik, M. D. Shirk, and B. C. Stuart: J. Appl. Phys., 102, (2007) 073112.

(Received: July 11, 2025, Accepted: October 25, 2025)